An adaptive LQG control for semi-active suspension systems

Hyun-Chul Sohn and Kyung-Tae Hong

Department of Mechanical and Intelligent Systems Engineering,
Pusan National University, San 30 Jangjeon dong, Kumjeong-ku,
Busan, 609-735, Korea
E-mail: hcson@pusan.ac.kr E-mail: hongkt@pusan.ac.kr

Keum-Shik Hong* and Wan-Suk Yoo

School of Mechanical Engineering, Pusan National University,
San 30 Jangjeon-dong, Kumjeong-ku, Busan 609-735, Korea
Fax: 82 (51) 514-0685
E-mail: kshong@pusan.ac.kr
*Corresponding author

Abstract: In this paper, a road-adaptive LQG control for the semi-active Macpherson strut suspension system of hydraulic type is investigated. A new control-oriented model, which incorporates the rotational motion of the unsprung mass, is introduced. A semi-active suspension controller adapting to road variations is proposed. First, based on the extended least squares estimation algorithm, a LQG controller adapting to the estimated road characteristics is designed. Through the computer simulations, the performance of the proposed semi-active suspension is compared with that of a non-adaptive one. The results show better control performance of the proposed system over the compared one.

Keywords: Macpherson strut suspension; semi-active suspension; road variations; identification; LQG control.

Reference to this paper should be made as follows: Sohn, H.-C., Hong, K.-T., Hong, K.-S. and Yoo, W.-S. (2004) 'An adaptive LQG control for semi-active suspension systems', *Int. J. Vehicle Design*, Vol. 34, No. 4, pp.309–326.

Biographical notes: Hyun-Chul Sohn received his B.S. degree from the School of Mechanical Engineering and the M.S. degree from the Department of Mechanical and Intelligent Systems Engineering in 1998 and 2000, respectively, at Pusan National University. He is now a Ph.D. candidate in the Department of Mechanical and Intelligent Systems Engineering. He is a member of ICASE. His research interests include adaptive control, system identification, vehicle control, and nonlinear systems theory.

Kyung-Tae Hong received his B.S. degree in electronic communication engineering from Kumoh National Institute of Technology, Gumi, Korea, in 2000 and the M.S. degree in mechatronics engineering from Pusan National University, Pusan, Korea, in 2002. He is now a Ph.D. candidate in the Department of Mechanical and Intelligent Systems Engineering at Pusan National University, Pusan, Korea. He is a member of ICASE. His research interests include adaptive control, crane control, suspension control, ECU development, and embedded systems.

Keum-Shik Hong received his B.S. degree in mechanical design and production engineering from Seoul National University in 1979, the M.S. degree in mechanical engineering from Columbia University, New York, in 1987, and both the M.S. degree in applied mathematics and the Ph.D. degree in mechanical engineering from the University of Illinois at Urbana-Champaign in 1991. Since Dr. Hong joined the School of Mechanical Engineering at Pusan National University, Korea, in 1993, he is now Associate Professor. During 1982-85, he was with Daewoo Heavy Industries, Incheon, Korea, where he worked on vibration, noise, and emission problems of vehicles and engines.

Dr. Hong serves as Associate Editor for Automatica (2000-date) and as Editor for the International Journal of Control, Automation, and Systems (2003-date). He is a member of ASME, IEEE, KSME, KSPE, and ICASE. Dr. Hong's current research interests include nonlinear systems theory, adaptive control, distributed parameter system control, input shaping, vehicle control, and innovative control applications to engineering problems.

Dr. Wan-Suk Yoo received his B.S. degree in mechanical engineering from Seoul National University in 1976, the M.S. degree in mechanical engineering from Korea Advanced Institute of Science and Technology in 1978, and Ph.D. degree in mechanical engineering from the University of Iowa, USA, in 1985, respectively. He joined the School of Mechanical Engineering, Pusan National University, in 1979 and is currently a professor. He served as Associate Dean of College of Engineering at Pusan National University during 1994-1996. Dr. Yoo is the Director of the Mechanical Engineering and Technology Research Information Centre, Korea. His research interests include kinematics, multibody dynamics, and vehicle dynamics.

1 Introduction

The roles of a suspension system are to support the vehicle weight, to isolate the vehicle body from road disturbances, and to maintain the traction force between the tyre and the road surface. Suspension systems are classified into a passive system and an active system according to the existence of control input. The active suspension system can be further classified into two types: a semi-active system and a fully active system according to the control input generation mechanism. Semi-active suspension systems are getting more attention because of their low cost and competitive performance to fully active ones. In this paper, a road-adaptive LQG control for the semi-active Macpherson strut suspension system of hydraulic type is investigated.

The performance of a suspension system is characterised by the ride quality, the handling performance of vehicle, the size of the rattle space, and the dynamic tyre force. The prime purpose of adopting an active/semi-active suspension system is to improve the ride quality and the handling performance of vehicle [1–9]. For a fixed suspension spring constant, a soft damping achieves the better isolation of the sprung mass from road disturbances by allowing a larger suspension deflection. However, the better road contact can be achieved with a hard damping by not allowing unnecessary suspension deflections. Therefore, the ride quality and the handling performance of vehicle are two conflicting criteria in the control system design of suspension systems [4,10,11].

In this paper, assuming the use of one acceleration sensor for each quarter-car model, a road-adaptive LQG control is pursued: First, a new control-oriented model for the

semi-active Macpherson suspension system is used. Second, a controller structure involving the estimation of road conditions using the extended least squares estimation method is suggested. Third, a LQG control using estimated road profiles is developed. One final comment is that the use of total four acceleration sensors (three vertical sensors and one lateral sensor) for the entire vehicle control is suggested, but the issues beyond a quarter-car model are not discussed in this paper.

2 A quarter-car model

A schematic diagram for controlling the Macpherson strut suspension system including its quarter-car model is shown in Figure 1. The quarter-car model admits the rotational motion of the unsprung mass. For the brevity of this paper, the detailed assumptions made for this model are referred to [4]. If the mass of the control arm is neglected and the bushing is assumed to be a pin joint, then its degree-of-freedom is two: z_s and θ, where z_s is the vertical displacement of the sprung mass and θ is the angular displacement of the unsprung mass. In this section, the derivation in [4] is modified to fit to the control problem of the semi-active suspension system with a continuously variable damper.

Figure 1 A new model for the semi-active Macpherson suspension

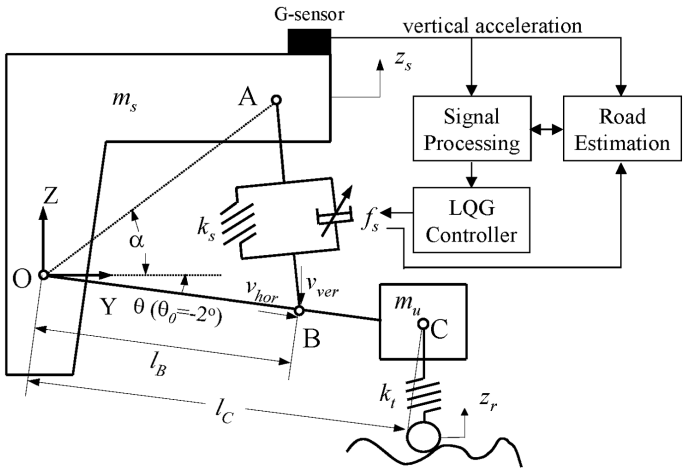

For the two generalised coordinates z_s and θ, the equations of motion become:

$$(m_s+m_u)\ddot{z}_s + m_u l_C \cos(\theta-\theta_0)\ddot{\theta} - m_u l_C \sin(\theta-\theta_0)\dot{\theta}^2 + k_t\left\{z_s + l_C\left(\sin(\theta-\theta_0)-\sin(\theta_0)\right)-z_r\right\}=0, \tag{1}$$

$$m_u l_C^2\ddot{\theta} + m_u l_C \cos(\theta-\theta_0)\ddot{z}_s + k_t l_C \cos(\theta-\theta_0)\left\{z_s + l_C\left(\sin(\theta-\theta_0)-\sin(-\theta_0)\right)-z_r\right\} - \frac{1}{2}k_s \sin(\alpha'-\theta)\left\{b_l + \left[d_l \Big/ \left(c_l - d_l \cos(\alpha'-\theta)^{\frac{1}{2}}\right)\right]\right\} = -l_B f_s, \tag{2}$$

where $a_l = l_A^2 + l_B^2$, $b_l = 2l_A l_B$, $\alpha' = \alpha + \theta_0$,

$c_l = a_l^2 - a_l b_l \cos(\alpha')$ and $d_l = a_l b_l - b_l^2 \cos(\alpha')$.

The parameters in Figure 1 are collected in Table 1.

Table 1 Vehicle parameters

Parameters	*Descriptions*	*Values*
m_s	Sprung mass	453 Kg
m_u	Unsprung mass	36 Kg
k_s	Coil spring constant	17,658 N/m
k_t	Tyre spring constant	183,887 N/m
l_A	Distance from O to A	0.66 m
l_B	Distance from O to B	0.34 m
l_C	Control arm length	0.37 m
α	Angle of OA	74
θ_0	Initial angle of control arm	–2

Now, let the state variables be $[x_1\ x_2\ x_3\ x_4]^{\mathrm{T}} = \left[z_s\ \dot{z}_s\ \theta\ \dot{\theta}\right]^{\mathrm{T}}$ and let the output be $y = \ddot{z}_s$. The linearisation of (1)–(2) at an equilibrium point $x_e = (x_{1e}, x_{2e}, x_{3e}, x_{4e}) = (0, 0, \theta_0\ 0)$ yields:

$$\dot{x}(t) = A_m x(t) + B_1 f_s + B_2 z_r(t),\ x(0) = x_0, \tag{3}$$

$$y(t) = C_m x(t) + D_1 f_s + D_2 z_r, \tag{4}$$

where

$$A_m = \begin{bmatrix} 0 & 1 & 0 & 0 \\ a_{21} & 0 & a_{23} & 0 \\ 0 & 0 & 0 & 1 \\ a_{41} & 0 & a_{43} & 0 \end{bmatrix} = \begin{bmatrix} 0 & 1 & 0 & 0 \\ -0.49437 & 0 & 21.177 & 0 \\ 0 & 0 & 0 & 1 \\ -13796 & 0 & -5105.4 & 0 \end{bmatrix},$$

$$B_1 = \begin{bmatrix} 0 \\ \dfrac{l_B \cos(-\theta_0)}{m_s l_C + m_u l_C \sin^2(-\theta_0)} \\ 0 \\ -\dfrac{(m_s + m_u) l_B}{m_s m_u l_C^2 + m_u^2 l_C^2 \sin^2(-\theta_0)} \end{bmatrix} = \begin{bmatrix} 0 \\ 0.002 \\ 0 \\ -0.074 \end{bmatrix},$$

$$B_2 = \begin{bmatrix} 0 \\ \dfrac{k_t l_C \sin^2(-\theta_0)}{m_s l_C + m_u l_C \sin^2(-\theta_0)} \\ 0 \\ \dfrac{m_s k_t l_C \cos(-\theta_0)}{m_s m_u l_C^2 + m_u^2 l_C^2 \sin^2(-\theta_0)} \end{bmatrix} = \begin{bmatrix} 0 \\ 0.494 \\ 0 \\ 13,796 \end{bmatrix},$$

$$C_m = \begin{bmatrix} a_{21} & 0 & a_{23} & 0 \end{bmatrix},$$

$$D_1 = \left[\frac{l_B \cos(-\theta_0)}{m_s l_C + m_u l_C \sin^2(-\theta_0)} \right] = \begin{bmatrix} 0.002 \end{bmatrix},$$

$$D_2 = \left[\frac{k_t l_C \sin^2(-\theta_0)}{m_s l_C + m_u l_C \sin^2(-\theta_0)} \right] = \begin{bmatrix} 0.494 \end{bmatrix},$$

and see [5] for the expressions of a_{21}, a_{23}, a_{41}, and, a_{43}.

3 Road adaptation

The control objectives are the improvement of both the ride quality and the handling performance of vehicle. If fixed control gains are used, these two conflicting objectives cannot be achieved. However, by adapting road conditions, i.e., by changing controller gains for various road conditions, both objectives can be selectively achieved [10,11]. In this paper, as shown in Figure 2, a LQG control with road adaptation, in the form of an output feedback control, is proposed.

Figure 2 Road adapting semi-active control system

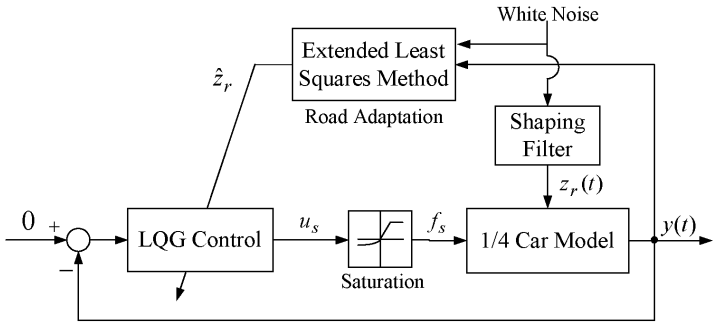

3.1 Road profiles

The power spectral density of a road surface is assumed given in the following form [3,6,12].

$$S_v(v) = \frac{\sum_{j=0}^{m} b_{vj} v^{2j}}{\sum_{i=0}^{n} a_{vi} v^{2i}}, \tag{5}$$

where v is the spatial frequency [cycle/m] of the road surface, and a_{vi}, b_{ij} are the parameters to be shaped. When a vehicle is moving along the road with velocity V, the excitation frequency of the road input ω [rad/s] becomes $\omega = 2\pi vV$. The mean squared value of road surface roughness, that is the total area of the power spectral density function, does not change with the velocity of a vehicle. Therefore we have the following relation:

$$S_r(\omega)\mathrm{d}\omega = S_v(v)\mathrm{d}v, \tag{6}$$

where $S_r(\omega)$ represents the power spectral density of a road input with respect to the displacement excitation frequency. We can express the power spectral density of a road input using the relationship $\mathrm{d}v = (2\pi V)^{-1}\mathrm{d}\omega$ as

$$S_r(\omega) = \frac{\sum_{j=0}^{m} b_{vj} (2\pi V)^{-2j-1} \omega^{2j}}{\sum_{i=0}^{n} a_{vi} (2\pi V)^{-2i} \omega^{2i}}. \tag{7}$$

We now determine the transfer function $G_r(j\omega) = z_r(t)/\varepsilon(t)$ where $\varepsilon(t)$ is the input white noise and $z_r(t)$ is the actual road profiles, of the shaping filter, so that the power spectral density of the output coloured noise of the shaping filter is the same as that of the actual road surface. The relationship between the two power spectral densities is represented as

$$S_r(\omega) = \left|G_r(\omega)\right|^2 S_\varepsilon(\omega), \tag{8}$$

where $S_e(\omega)$ is the normalised power spectral density function of white noise. Therefore, the transfer function of the shaping filter can be determines as

$$G_r(s) = \sqrt{(2\pi V)^{2n-2m-1}} \frac{\sqrt{b_{vm}} \prod_{j=0}^{m} (s - z_j)}{\sqrt{a_{vm}} \prod_{i=0}^{n} (s - p_i)}, \tag{9}$$

where p_i and z_j are negative roots of the following equations:

$$\sum_{i=0}^{n} (-1)^i a_{vi} (2\pi V)^{-2i} s^{2i} = 0, \tag{10}$$

$$\sum_{j=0}^{m} (-1)^j b_{vj} (2\pi V)^{-2j-1} s^{2j} = 0. \tag{11}$$

By increasing the orders (m, n) in (5), the statistical properties of road input will be increased. However, the increase of the orders will increase the calculation time, which may deteriorate the overall control performance. In this paper, $m = 1$, and $n = 2$ are used.

3.2 Extended least squares estimation

The shaping filter of (9) can be rewritten in the following ARMA (auto-regressive moving averages) model with respect to input white noise $\varepsilon(t)$ by using the zero-order holder and z-transform.

$$G_r(z^{-1}) = \frac{z_r(t)}{\varepsilon(t)} = \frac{1 + b_{k_1} z^{-1} + b_{k_2} z^{-2}}{1 + a_{k_1} z^{-1} + a_{k_2} z^{-2}}. \tag{12}$$

The ARMA model can be rewritten in the following regression form:

$$z_r(t) = \Phi^{\mathrm{T}}(t-1)\theta + \varepsilon(t), \tag{13}$$

where θ is the parameter vector to be estimated and $\Phi(t-1)$ includes all known variables as

$$\theta = \begin{bmatrix} a_{k_1} & a_{k_2} & b_{k_1} & b_{k_2} \end{bmatrix}^{\mathrm{T}}, \tag{14}$$

$$\Phi(t-1) = [-z_r(t-1) \;\; -z_r(t-2) \;\; \varepsilon(t-1) \;\; \varepsilon(t-2)]^{\mathrm{T}}. \tag{15}$$

The estimated output $\hat{z}_r(t)$ is denoted as

$$\hat{z}_r(t) = \Phi^{\mathrm{T}}(t-1)\hat{\theta}(t). \tag{16}$$

The parameter vector $\hat{\theta}$ should be chosen to minimise the least squares loss function J_{LS} in terms of the estimated error $e_s(t) = z_r(t) - \hat{z}_r(t)$

$$J_{LS}(\hat{\theta}, t) = \frac{1}{2}\sum_{i=1}^{t} \lambda^{t-i} \{z_r(i) - \Phi^{\mathrm{T}}(i-1)\hat{\theta}(i)\}^2, \tag{17}$$

where λ, $0 < \lambda \le 1$, is the forgetting factor. In this work, $\lambda = 0.9$ is used. If $\Phi(t-1)$ has full rank, then the least squares estimate $\hat{\theta}(t)$ satisfies the recursive equations

$$\hat{\theta}(t) = \hat{\theta}(t-1) + L(t)\left[z_r(t) - \Phi^{\mathrm{T}}(t)\hat{\theta}(t-1)\right], \tag{18}$$

$$L(t) = \frac{P(t-1)\Phi(t)}{\lambda + \Phi^{\mathrm{T}}(t)P(t-1)\Phi(t)}, \tag{19}$$

$$P(t) = \frac{1}{\lambda}\left\{I - L(t)\Phi^{\mathrm{T}}(t)\right\}P(t-1). \tag{20}$$

In this paper, the first two terms in (15) are obtained from the measured data $\ddot{z}_s$. The transfer function from $z_r(s)$ to $\ddot{z}_s(s)$ is derived from (3) and (4) as follows:

$$\begin{aligned} G_{rs}(s) &\overset{\Delta}{=} \frac{\ddot{z}_s(s)}{z_r(s)} = C'(sI - A')^{-1}B_2 + D_2 \\ &= \frac{0.5s^4 + 17212.4s^3 + 317325s^2 - 11.5s - 212.6}{s^4 + 45.7s^3 + 509765s^2 + 17212.4s + 317359}, \end{aligned} \tag{21}$$

where A′ = A + B_1H, C′ =C + D_1H, (A, B_2, C, D_2) are from (3)–(4), and H satisfies

$$f_s = c_p \dot{\Delta l} \cong Hx \text{, where } H \overset{\Delta}{=} c_p \left[0 \;\; 0 \;\; \partial \dot{\Delta l}/\partial\theta \;\; \partial \dot{\Delta l}/\partial \dot{\theta} \right]_{(0,\,0,\,\theta_0,\,0)}.$$

It is noted that H has been introduced to avoid possible roots on the imaginary axis. In this work, H = [0 0 0 614] has been used. Therefore, using the transfer function above, the road input can be estimated as follows:

$$z_r(s) = \frac{40\pi}{s + 40\pi} G^{-1}{}_{rs}(s)\, \ddot{z}_s(s), \tag{22}$$

where a low-pass filter of cutoff frequency 20 Hz has been added to enhance the stability of the filter.

The last two terms in (15) are approximated by using (13) and (16) as follows:

$$\varepsilon(t) \cong \zeta(t) = z_r(t) - \Phi^{\mathrm{T}}(t-1)\hat{\theta}(t). \tag{23}$$

Finally, $\Phi(t-1)$ takes the form

$$\Phi(t-1) = \left[-z_r(t-1) \;\; -z_r(t-2) \;\; \zeta(t-1) \;\; \zeta(t-2) \right]^{\mathrm{T}}. \tag{24}$$

4 A road-adaptive LQG control

In this section, by incorporating the estimated road roughness in the performance index, a road adaptive LQG controller is designed. The control objective is achieved by letting the semi-active suspension system to track the control force calculated in the LQG controller.

4.1 LQG control

In Figure 3, the transfer function $W(z^{-1})$ from f_s to y and the transfer function $W_d(z^{-1})$ from z_r to y are obtained by z-transforming (3)–(4), with sampling time 0.01 sec, as follows:

Figure 3 Output feedback control system

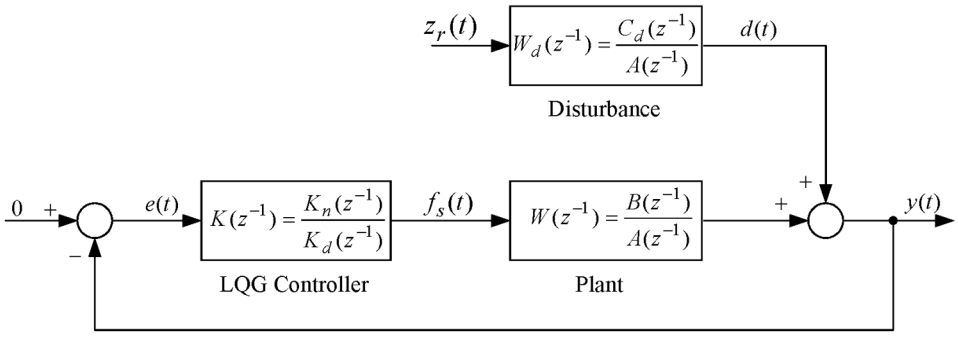

$$W(z^{-1}) = \frac{y(t)}{f_s(t)} \triangleq \frac{B(z^{-1})}{A(z^{-1})}, \tag{25}$$

$$W_d(z^{-1}) = \frac{y(t)}{z_r(t)} \triangleq \frac{C_d(z^{-1})}{A(z^{-1})}. \tag{26}$$

It is noted that $W(z^{-1})$ must not contain unstable modes and $W_d(z^{-1})$ should be asymptotically stable. Also, the white noise $\varepsilon(t)$ is assumed to be $N(0, \sigma^2)$. Let $S(z^{-1})$ and $M(z^{-1})$ be the sensitivity function and the control sensitivity function, respectively, as follows:

$$S(z^{-1}) = \frac{y(t)}{d(t)} = \frac{1}{1+W(z^{-1})K(z^{-1})}, \tag{27}$$

$$M(z^{-1}) = -\frac{u_s(t)}{d(t)} = \frac{K(z^{-1})}{1+W(z^{-1})K(z^{-1})}. \tag{28}$$

The performance index is defined as follows:

$$\begin{aligned} J &= \frac{1}{2\pi \mathrm{j}} \oint_{|z|=1} X(z^{-1}) \frac{\mathrm{d}z}{z} \\ &= \frac{1}{2\pi \mathrm{j}} \oint_{|z|=1} \left\{ Q_c \Phi_{ee} + R_c \Phi_{uu} + G_c \Phi_{ue} + G_c^* \Phi_{eu} \right\} \frac{\mathrm{d}z}{z}. \end{aligned} \tag{29}$$

where * denotes the adjoint, Q_c, R_c, and G_c are dynamic weightings given by

$$Q_c = \frac{B_q^* B_q}{A_q^* A_q}, \; R_c = \frac{B_r^* B_r}{A_r^* A_r}, \; G_c = \frac{B_q^* B_r}{A_q^* A_r}. \tag{30}$$

For the sake of brevity, the arguments of shift operators are suppressed. In equation (29), Φ_{uu}, Φ_{ee}, and Φ_{ue} are the power spectra of control $f_s(t)$, error $e(t)$, and cross-weighting terms, respectively, as

$$\Phi_{uu} = M \Phi_{dd} M^*, \tag{31}$$

$$\Phi_{ee} = S \Phi_{dd} S^*, \tag{32}$$

$$\Phi_{ue} = M^* \Phi_{dd} S, \tag{33}$$

where Φ_{dd} denotes the power spectrum of the disturbance as

$$\Phi_{dd} = Y_f^* Y_f = \left\{ \frac{C_d}{A} \varepsilon(t) \right\}^* \left\{ \frac{C_d}{A} \varepsilon(t) \right\} = \frac{C_d^* C_d}{A^* A}. \tag{34}$$

Substituting (31)–(34) into (29) yields:

$$\begin{aligned} X(z^{-1}) = Y_f^* [& M^* (W^* Q_c W + R_c - W^* G_c - G_c^* W) M + Q_c \\ & - M^* W^* Q_c - Q_c W M + M G_c + M^* G_c^*] \; Y_f. \end{aligned} \tag{35}$$

This equation suggests that the following spectral factors are defined:

$$Y_c^* Y_c = W^* Q_c W + R_c - W^* G_c - G_c^* W, \tag{36}$$

$$\Phi_h = W^* \Phi_{dd} Q_c - G_c^* \Phi_{dd} . \tag{37}$$

Hence, the substitution of (36) and (37) into (35) gives:

$$\begin{aligned} X &= Y_f^* [M^* (W^* Q_c W + R_c - W^* G_c - G_c^* W) M + Q_c - M^* W^* Q_c - Q_c W M + M G_c + M^* G_c^*] Y_f \\ &= (Y_c M Y_f - Y_c^{*-1} \Phi_h Y_f^{*-1})^* (Y_c M Y_f - Y_c^{*-1} \Phi_h Y_f^{*-1}) + Q_c \Phi_{dd} - Y_c^{*-1} \Phi_h Y_f^{*-1} Y_f^{-1} \Phi_h^* Y_c^{-1}. \end{aligned} \tag{38}$$

The spectral factor $Y_c^* Y_c$ is defined by substituting (25) and (30) into (29).

$$Y_c^* Y_c = \frac{D_c^* D_c}{A A^* A_q A_q^* A_r A_r^*} . \tag{39}$$

Using (39), the terms of (38) are derived, respectively, as

$$Y_c M Y_f = \frac{D_c C_d K_n}{A A_q A_r (A K_d + B K_n)} , \tag{40}$$

$$Y_c^{*-1} \Phi_h Y_f^{*-1} = \frac{B_q C_d (A_r^* B^* B_q^* - A^* A_q^* B_r^*)}{D_c^* A A_q} . \tag{41}$$

4.2 Optimisation problem

It is necessary to introduce several Diophantine equations to simplify the polynomial expression. The term in (41) can be written as a partial-fraction expansion, in terms of the solution G and F, of the following Diophantine equation:

$$D_c^* G z^{-g} + F A A_q = B_q C_d (A_r^* B^* B_q^* - A A_q^* B_r^*) z^{-g} , \tag{42}$$

where g is the smallest value which ensures the terms of (42) to involve only polynomials in z^{-1}, whereas D_c^*, for example, is a polynomial in z.

Attention may now return to the optimisation argument based on (38). The first term in (38) is expressed as

$$Y_c M Y_f - Y_c^{*-1} \Phi_h Y_f^{*-1} = \frac{D_c C_d K_n}{A A_q A_r (A K_d + B K_n)} - \frac{G}{A A_q} - \frac{F z^g}{D_c^*} . \tag{43}$$

A second Diophantine equation is required to calculate $D_c C_d$ in (43). The equation follows in terms of the solution polynomials H and F, where F also arose in (42):

$$D_c^* A_r H z^{-g} - F B A_r A_q = (B_r B_r^* A^* A_q A_q^* - B^* B_q^* B_r A_q A_r^*) C_d z^{-g} \tag{44}$$

The adding of (42) and (44), appropriately multiplied, gives:

$$D_c^* (G A_r B + H A A_r) z^{-g} = D_c^* D_c C_d z^{-g} . \tag{45}$$

By cancelling the common D_c^* and z^{-g} in both sides of (45), D_cC_d is obtained as

$$GA_rB + HAA_r = D_cC_d\,. \tag{46}$$

Substituting (46) into (43) gives:

$$Y_cMY_f - Y_c^{*-1}\Phi_hY_f^{*-1} = \frac{HK_n - GK_d}{A_q(AK_d + BK_n)} - \frac{Fz^g}{D_c^*}\,. \tag{47}$$

Thus, the expression (47) has been separated into a causal and non-causal terms. The only term in the performance index (29) which depends upon the controller K is the first causal term. It follows that the performance index is minimised when the first causal term is zero.

$$K = \frac{K_n}{K_d} = \frac{G}{H}\,. \tag{48}$$

Hence, the desired control force is determined as

$$u_s(t) = -Ky(t)\,, \tag{49}$$

where K is defined in (48).

4.3 Selection of dynamic weighting

The control-gain of the LQG controller is determined by adjusting the dynamic weight in (30). In this paper, the dynamic weights such as $Q_c(z^{-1})$, $R_c(z^{-1})$, $G_c(z^{-1})$ are determined by considering the road roughness and the characteristics of human response to acceleration. The road roughness is determined by identifying the parameters of shaping filters in Section 2. Also, human response characteristics are to use the concept of the equivalent weighting filter to human response to vibrations suggested by Jang and Griffin [13]. Table 2 shows the weighting functions (BS6841) to assess human exposure to whole-body vibration, and Figure 4 shows approximation of frequency response characteristics to similar filters. The weighting functions to assess human response are considering the curve in Figure 4.

$$F(s) = \frac{s^2 + f_1s + f_2}{s^2 + f_3s + f_4}\,. \tag{50}$$

(50) is expressed as discrete transfer function as follows:

$$F(z^{-1}) = \frac{B_f(z^{-1})}{A_f(z^{-1})} = \frac{1 + b_{f_1}(z^{-1}) + b_{f_2}(z^{-1})}{1 + a_{f_1}(z^{-1}) + a_{f_2}(z^{-1})}\,. \tag{51}$$

Therefore, the dynamic weightings are as follows considering the road roughness (12) and human response characteristics (51).

$$Q_c(z^{-1}) = \frac{B_q^*(z^{-1})B_q(z^{-1})}{A_q^*(z^{-1})A_q(z^{-1})} = \frac{B_f^*(z^{-1})B_k^*(z^{-1})B_k(z^{-1})B_f(z^{-1})}{A_f^*(z^{-1})A_k^*(z^{-1})A_k(z^{-1})A_f(z^{-1})}\,, \tag{52}$$

Table 2 Frequency characteristics of weighting functions $W_h(f)$ to assess human exposure to whole-body vibration (BS6841)

Exposure area	*Measure axis*	*Weighting function*	*Multiplying factor*	*Frequency response*
Seat	x_{seat}, y_{seat}	w_d	1.00	$0.5 < f < 2.0 : W_h(f) = 1.0$
				$2.0 < f < 80.0 : W_h(f) = 2.0/f$
	z_{seat}	w_b	1.00	$0.5 < f < 2.0 : W_h(f) = 0.4$
				$2.0 < f < 5.0 : W_h(f) = f/5.0$
				$5.0 < f < 16.0 : W_h(f) = 1.0$
				$16.0 < f < 80.0 : W_h(f) = 16/f$
	R_x	w_e	0.63	$0.5 < f < 1.0 : W_h(f) = 0.63$
				$1.0 < f < 5.0 : W_h(f) = 0.63/f$
	R_y	w_e	0.40	$0.5 < f < 1.0 : W_h(f) = 0.4$
				$1.0 < f < 5.0 : W_h(f) = 0.4/f$
	R_z	w_e	0.20	$0.5 < f < 1.0 : W_h(f) = 0.2$
				$1.0 < f < 5.0 : W_h(f) = 0.2/f$
Back	x_b	w_c	0.80	$0.5 < f < 8.0 : W_h(f) = 0.8$
				$8.0 < f < 80.0 : W_h(f) = 6.4/f$
	y_b	w_d	0.50	$0.5 < f < 2.0 : W_h(f) = 0.5$
				$2.0 < f < 80.0 : W_h(f) = 1.0/f$
	z_b	w_d	0.40	$0.5 < f < 2.0 : W_h(f) = 0.4$
				$2.0 < f < 80.0 : W_h(f) = 0.8/f$
Feet	x_f, y_f	w_b	0.25	$0.5 < f < 2.0 : W_h(f) = 0.1$
				$2.0 < f < 5.0 : W_h(f) = f/20.0$
				$0.5 < f < 16.0 : W_h(f) = 0.25$
				$16.0 < f < 80.0 : W_h(f) = 4.0/f$
	z_f	w_b	0.40	$0.5 < f < 2.0 : W_h(f) = 0.16$
				$2.0 < f < 5.0 : W_h(f) = f/12.5$
				$5.0 < f < 16.0 : W_h(f) = 0.4$
				$16.0 < f < 80.0 : W_h(f) = 6.4/f$

Figure 4 Frequency characteristics of equivalent filters to weighting functions to assess human response to vibration

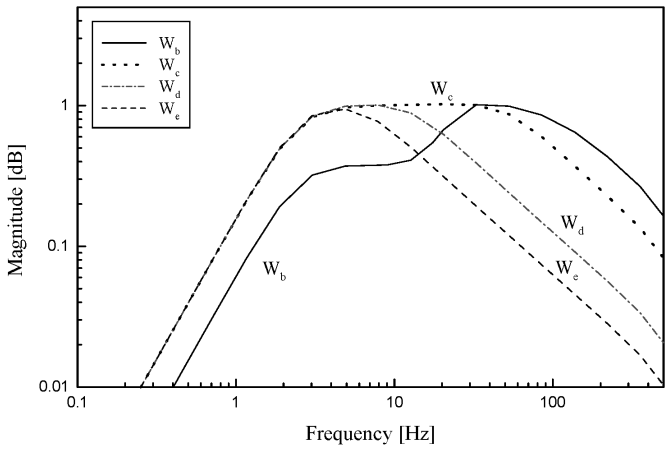

$$R_c(z^{-1}) = \frac{B_r^*(z^{-1})B_r(z^{-1})}{A_r^*(z^{-1})A_r(z^{-1})} = \frac{\rho^2\ B_f^*(z^{-1})B_k^*(z^{-1})B_k(z^{-1})B_f(z^{-1})}{A_f^*(z^{-1})A_k^*(z^{-1})A_k(z^{-1})A_f(z^{-1})}, \tag{53}$$

$$G_c(z^{-1}) = \frac{B_q^*(z^{-1})B_r(z^{-1})}{A_q^*(z^{-1})A_r(z^{-1})} = \frac{\rho\ B_f^*(z^{-1})B_k^*(z^{-1})B_k(z^{-1})B_f(z^{-1})}{A_f^*(z^{-1})A_k^*(z^{-1})A_k(z^{-1})A_f(z^{-1})}. \tag{54}$$

4.4 Continuously variable damper

Even though the computation of control input is carried out by (49), the actual control input is supplied by a continuously variable damper. Therefore, because of saturation, the actual force is limited as follows:

$$f_s = \begin{cases} f_s^*, & \text{if} \quad f_s^* \le u_s \\ u_s, & \text{if} \quad f_{s*} < u_s < f_s^* \\ f_{s*} & \text{if} \quad f_{s*} \ge u_s \end{cases} \tag{55}$$

where f_s^* and f_{s*} denote the maximum and the minimum damping forces available at a given relative velocity. With this control law, the actuator saturation would be unavoidable. Therefore, the control performance of a semi-active damper would be less perfect in severe road conditions.

The characteristics of a typical continuously variable damper are depicted in Figure 5. The solid line in the middle section denotes the damping force characteristics of a typical passive damper. The dotted line of highest slope denotes the characteristics for 0 amp current input, which is the most hard case. The triangles overlaid on top of the dotted line represent the lookup table values of the maximum damping force. The dotted line of lowest slope denotes the minimum damping force characteristics for 1.6 amp current input. Again, the squares denote the lookup table values of the minimum damping force. The damping forces in the extension region (the first quarter in Figure 5) are larger than those in the compression region (the third quarter).

Figure 5 Damping force characteristics of a typical continuously variable damper

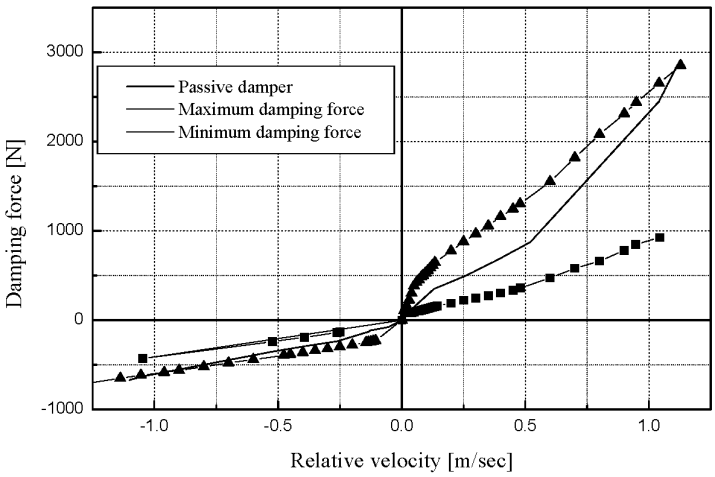

4.5 Current generation

The damping force generated in the actual damper depends on two things: the size of valve opening, i.e. the current input to the solenoid valve, and the relative velocity of the rattle space. To determine the current input to the solenoid valve, it is necessary to know the damping force characteristics of the valve vs. the current input at given relative velocity. For this, two approaches can be pursued. One is an analytic approach, which investigates the dynamics of the entire hydraulic system including the cylinder and valves. However, the mechanism of a semi-active system is very complicated and the damping force characteristics of expansion and compression strokes are different because of the one-sided piston rod. It is also difficult to measure the parameter values of the hydraulic system and furthermore these values are time varying. Another approach is an experimental solution, which is more or less straightforward. The damping forces for various input currents at given relative velocity can be measured with a test rig. In this paper, the experimental approach is adopted.

The experimental data can be either tabulated as a look-up table for the purpose of gain-scheduling or approximated as a polynomial equation by using the least squares method. After dividing the relative velocity range into four different sections, the polynomial equations corresponding to individual sections are tabulated in Table 3.

Table 3 Polynomial representation of maximum/minimum damping forces

	Maximum damping force [N]	*Minimum damping force* [N]
$0.25 < \dot{\Delta}l$	$440 + 1650\ \dot{\Delta}l + 420\ \dot{\Delta}l^2$	$95 + 405\ \dot{\Delta}l + 402\ \dot{\Delta}l^2$
$0 < \dot{\Delta}l < 0.25$	$8500\ \dot{\Delta}l - 36500\ \dot{\Delta}l^2 + 66450\ \dot{\Delta}l^3$	$37 + 1504\ \dot{\Delta}l - 7284\ \dot{\Delta}l^2 + 17164\ \dot{\Delta}l^3$
$-0.1 < \dot{\Delta}l < 0$	$6700\ \dot{\Delta}l + 78000\ \dot{\Delta}l^2 + 340000\ \dot{\Delta}l^3$	$530\ \dot{\Delta}l$
$\dot{\Delta}l < -0.1$	$410\ \dot{\Delta}l - 190$	$370\ \dot{\Delta}l - 16$

As far as final results are concerned, there is no much difference between these two methods. On the other hand, less calculation time is consumed with the polynomial approach. This is very important because the entire control algorithm should be coded in a microprocessor. Figure 6 compares the access times of the two methods when the relative velocity ranges within ± 1.4 m/s. It is seen that the calculation time of the polynomial equation is constant, but the access time needed to use the loop-up table increases as the number of data increases. In this work, the polynomial approximation approach is adopted.

The transformation algorithm block takes two inputs, the desired control force and the relative velocity of the rattle space and determines the duty ratio of the PWM generator. In our case, the duty ratio corresponding to 1.6 amp is 0.4 and that corresponding to 0 amp is 0. In this paper, the time constant of valve dynamics is ignored under the assumption that the solenoid valve response to a current input is instantaneous. Actually, the natural frequency of the solenoid valve used in this work is about 300 Hz.

Figure 6 Access time comparison: lookup table and polynomial

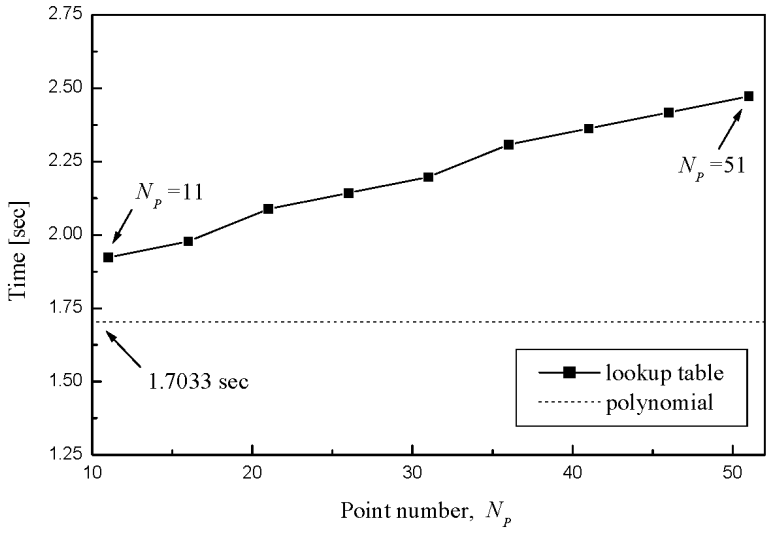

5 Simulations

Through computer simulations, the performance of the road-adaptive semi-active suspension system that takes into account of the road roughness Figure 7 is compared to that of a conventional semi-active suspension system (skyhook control) in Figure 8. The sampling time used during the system identification is 0.01 sec, and the initial values used for $P(t-1)$ and λ are $1 \times 10^6 I$ and 0.9, respectively.

Figure 7 Time history of road disturbance

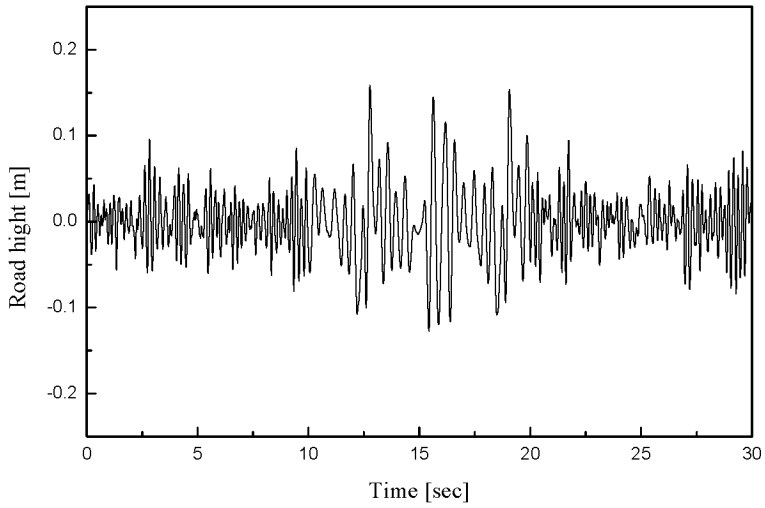

Figure 8 Acceleration responses of the sprung mass. (a) Comparison between the passive damper and the road adaptive LQG control, (b) Comparison between the conventional skyhook control and the road adaptive LQG control

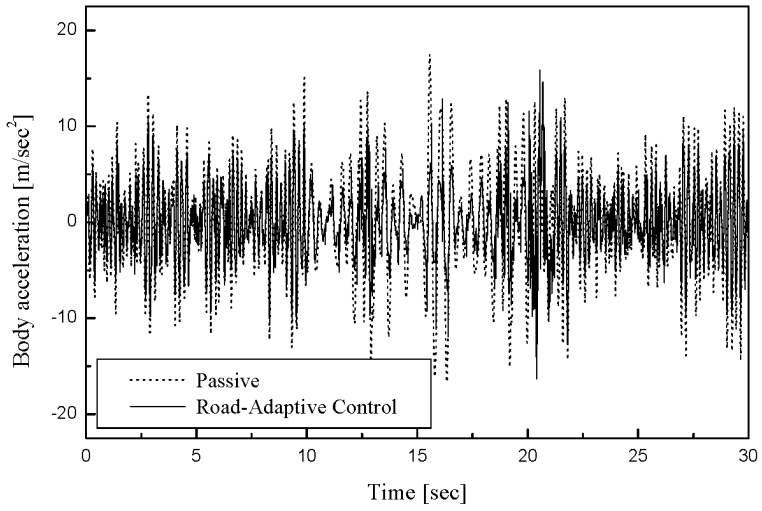

(a)

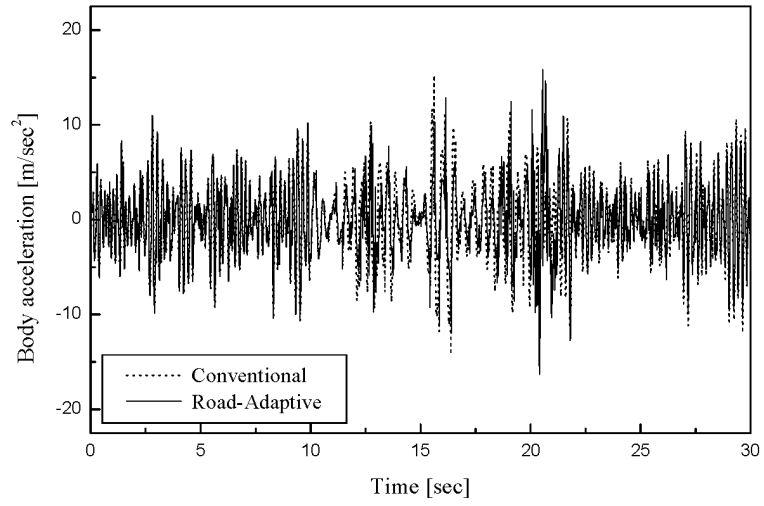

(b)

In Figure 8, the vehicle is driven on a paved road for 10 sec, a standard unpaved road for 10 sec, and again on a paved road for 10 sec, sequentially, at the speed of 60 km/h. Figure 8(a) compares the ride quality of the road-adaptive LQG control to that of a passive suspension system (c_p = 2,000 N s/m). Also, Figure 8(b) compares the ride quality of the road-adaptive LQG control to that of a conventional skyhook control. The root mean square (RMS) values for the road-adaptive LQG control, the conventional skyhook control, and the passive suspension system during the entire period are 4.49, 4.94 and 7.22 m/s^2, respectively. As can be noticed in Figure 8(b), for the first

10 sec, the vertical accelerations of the road-adaptive LQG control and the conventional skyhook control are similar, but the ride quality of the road-adaptive LQG control is superior to that of a conventional skyhook control when the vehicle reaches the unpaved road. During the unpaved road, the RMS values for the road-adaptive LQG control and the conventional skyhook control show much larger difference: 4.98 and 6.63 m/s^2, respectively.

6 Conclusions

In this paper, a road-adaptive LQG control for the semi-active Macpherson suspension system, by using a new control-oriented model, was investigated. The new model incorporates the rotational motion of the unsprung mass, giving a better description for the plant dynamics and keeping the degree-of-freedom of the plant model by two. Upon the requirement of using only one acceleration sensor, a LQG control with road adaptation was developed. Because the control law design and the road estimation method developed in this paper are not restricted to a particular suspension system, the entire strategy can be extended to any semi-active system including an ER damper and a MR damper.

Acknowledgments

This work was supported by the Ministry of Science and Technology of Korea under the program of National Research Laboratory, grant number NRL M1-0203-00-0017-02J0000-00910.

References

1 Hady, M.B.A.A. and Crolla, D.A. (1992) 'Active suspension control algorithms for a four-wheel vehicle model', *International Journal of Vehicle Design*, Vol. 13, No. 2, pp.144–158.

2 Alleyne, A. and Hedrick, J.K. (1995) 'Nonlinear adaptive control of active suspensions', *IEEE Transaction on Control Systems Technology*, Vol. 3, No. 2, pp.94–101.

3 Crolla, D.A. and Hady, M.B.A.A. (1991) 'Active suspension control: performance comparisons using control laws applied to a full vehicle model', *Vehicle System Dynamics*, Vol. 20, pp.107–120.

4 Hong, K.S., Jeon, D.S., Yoo, W.S., Sunwoo, H., Shin, S.Y., Kim, C.M. and Park, B.S. (1999) 'A new model and an optimal pole-placement control for the Macpherson suspension system', *SAE Paper*, No. 1999-01-1331, pp.267–276.

5 Hong, K.S., Sohn, H.C. and Hedrick, J.K. (2002) 'Modified skyhook control of semi-active suspensions: a new model, gain scheduling, and hardware-in-the-loop tuning', *ASME Transactions, Journal of Dynamic Systems, Measurement, and Control*, Vol. 124, No. 1, pp.158–167.

6 Jeong, W.B. (1990) 'State estimation of road surface and vehicle system using a kalman filter', *JSME International Journal, Series C: Mechanical Systems, Machine Elements and Manufacturing*, Vol. 33, No. 4, pp.528–534.

7 Karnopp, D.C., Crosby, M.J. and Harwood, R.A. (1974) 'Vibration control using semi-active force generators', *ASME Journal of Engineering for Industry*, Vol. 96, No. 2, pp.619–626.

8 Sharp, R.S. and Crolla, D.A. (1987) 'Road vehicle suspension system design: a review', *Vehicle System Dynamics*, Vol. 16, pp.167–192.

9 Sohn, H.C., Hong, K.S. and Hedrick, J.K. (2000) 'Semi-active control of the Macpherson suspension system: hardware-in-the-loop simulations', *IEEE International Conference on Control Application & IEEE International Symposium on CACSD*, WP4-6, pp.982–987.

10 Gordon, T.J. and Sharp, R.S. (1998) 'On improving the performance of automotive semi-active suspension systems through road preview', *Journal of Sound and Vibration*, Vol. 217, No. 1, pp.163–182.

11 Kim, H. and Yoon, Y.S. (1995) 'Semi-active suspension with preview using a frequency-shaped performance index', *Vehicle System Dynamics*, Vol. 24, pp.759–780.

12 Robson, J.D. (1979) 'Road surface description and vehicle response', *International Journal of Vehicle Design*, Vol. 1, No. 1, pp.25–35.

13 Jang, H.K. and Griffin, M.J. (1999) 'The effect of phase of differential vertical vibration at the seat and feet on discomfort', *Journal of Sound and Vibration*, Vol. 223, No. 5, pp.785–794.